Inorganic Chemistry

Article

pubs.acs.org/IC

The Inverse Trans Influence in a Family of Pentavalent Uranium Complexes

Andrew J. Lewis,[†] Kimberly C. Mullane,[†] Eiko Nakamaru-Ogiso,[‡] Patrick J. Carroll,[†] and Eric J. Schelter*[,†]

[†]P. Roy and Diana T. Vagelos Laboratories, Department of Chemistry and [‡]Department of Biochemistry and Biophysics, Perelman School of Medicine, University of Pennsylvania, Philadelphia, Pennsylvania 19104, United States

Supporting Information

ABSTRACT: Systematic ligand variation in a structurally conserved framework of pentavalent uranium complexes of the formulas $U^{V}X_2[N(SiMe_3)_2]_3$ (X = F, Cl, Br, N_3, NCS, 2-naphthoxide) and $U^{V}OX[N(SiMe_3)_2]_3^-$ (X = −CCPh, −CN) allowed an investigation into the role of the inverse trans influence in pentavalent uranium complexes. The −CCPh and −CN derivatives were only stable in the presence of the *trans*-U═O multiple bond, implicating the inverse trans influence in stabilizing these complexes. Spectroscopic, structural, and density functional theory calculated electronic structural data are explored. Near-IR data of all complexes is presented, displaying vibronic coupling of $5f^1$ electronic transitions along the primary axis. Electrochemical characterization allowed assessment of the relative donating ability of the various axial ligands in this framework. Electron paramagnetic resonance data presented display axial spectra, with hyperfine coupling along the primary axis.

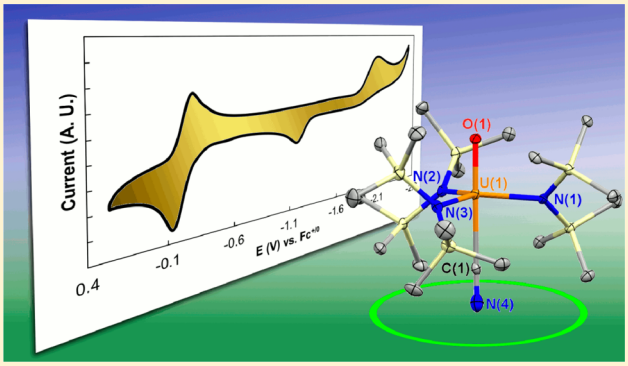

INTRODUCTION

The inverse trans influence (ITI) is a thermodynamic phenomenon that involves cooperative stabilization of metal−ligand bonds trans to one another in axially symmetric 5f complexes. The ITI is the key electronic structure feature in the chemistry of high-valent actinides[1,2] and underlies the stability of the "actinyl" ions, for example, AnO_2^{n+}. Recent work from several groups,[3−9] including ours,[10−12] has included investigations into the origin of ITI stabilization, toward the goal of enabling the synthesis of reactive uranium−ligand bonds. Most of the work in this area has focused on uranium(VI) complexes. Although structural evidence for ITI stabilization has been inferred in uranium(V) complexes,[13] the importance of the ITI in axial uranium(V) complexes and effects on their electronic structures are currently unknown.[10]

Pentavalent uranium is the ideal electronic configuration to probe electronic structure effects in the study of axial complexes. The electronic structure that results from the $5f^1$ configuration is relatively simple compared to larger $5f^n$ electron counts because of the absence of inter 5f-electron repulsion.[14] Analyses of crystal field effects and spin−orbit coupling in uranium(V) complexes have been successful based on simple, symmetric complexes.[15,16] Comparison of the σ- and π-donating ability of alkoxide,[17] amide,[18] alkyl,[19] and ketimide[20] ligands was achieved through the preparation of the six-coordinate, homoleptic uranium(V) complexes.[15] However, routes to synthesizing families of structurally related heteroleptic uranium(V) complexes are rare.[21] High-valent uranium complexes are typically stabilized by multiply bonded ligands[22] and, particularly in the case of pentavalent uranyl complexes, require steric protection to prevent disproportionation.[23,24]

Chart 1. Structurally Related Uranium(V) Complexes That Were Previously Reported[10]

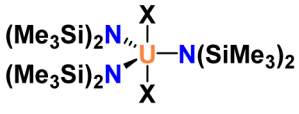

1-X

X = F^-, Cl^-, Br^-, N_3^-, NCS^-, F^-/Cl^-

In this work, we extend our previously reported synthetic methods to prepare complexes of the formula $UX_2[N(SiMe_3)_2]_3$ (Chart 1) to include an aryloxide derivative and discuss our attempts to prepare cyanide and phenylacetylide derivatives, which were only successful in the presence of the strongly ITI-stabilizing oxo ligand. Furthermore, we present experimental and theoretical data on the series of uranium(V) complexes in an effort to elucidate the role of the ITI in axial, pentavalent uranium complexes.

RESULTS AND DISCUSSION

Synthesis of $U^{V}X_2[N(SiMe_3)_2]_3$ Complexes (1-X). We recently communicated methods for the synthesis of a series of trigonal bipyramidal pentavalent uranium complexes of the formula (Chart 1) $UX_2[N(SiMe_3)_2]_3$ (**1-X**).[10] This methodology allowed the preparation of several uranium(V) complexes, including **1-F**, **1-Cl**, **1-Br**, **1-N_3**,[25] **1-NCS**, and **1-FCl**, through oxidation

Received: April 11, 2014
Published: June 10, 2014

   dx.doi.org/10.1021/ic500833s | *Inorg. Chem.* 2014, 53, 6944−6953

and salt metathesis reactions. In the current work, an additional new derivative of **1-X** was synthesized and characterized.

Addition of 3 equiv of K(2-naphthoxide) (KONap) to a tetrahydrofuran (THF) solution of **1-Cl** led to a color change from dark red to orange, with formation of a product that was tentatively assigned by ^{1}H NMR spectroscopy as $[K(THF)_n][U^{IV}(ONap)_2[N(SiMe_3)_2]_3]$ (Supporting Information, Figure S1). Despite the formal reduction of the uranium ion in this reaction, no obvious oxidation product was identified. The uranium(IV) complex formed in situ was not isolated, but was treated with 4 equiv of $CuBr_2$, resulting in rapid color change to dark red (Scheme 1a). Extraction and recrystallization from Et_2O afforded $U^V(ONap)_2[N(SiMe_3)_2]_3$ **1-ONap** as a black crystalline solid.

Scheme 1. Synthesis of 1-ONap and Attempted Syntheses of Other 1-X Derivatives

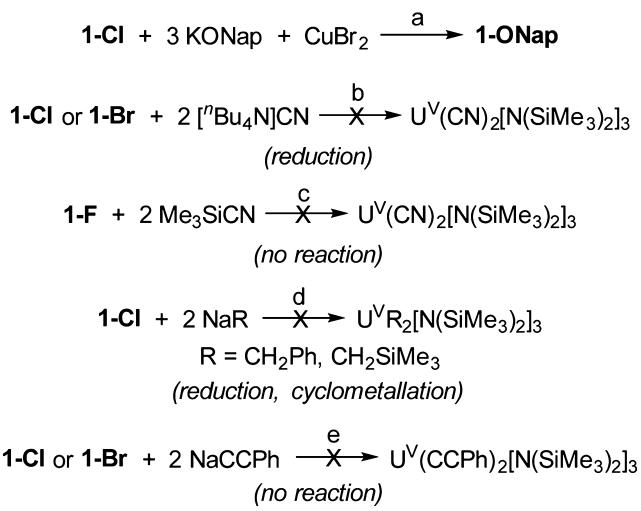

The X-ray crystal structure of **1-ONap** displays an unusual structural distortion relative to the approximately D_3 symmetric arrangement in the other **1-X** complexes (Figure 1). The Si−N−Si plane of one of the $N(SiMe_3)_2^-$ ligands is forced into the equatorial plane of the complex to accommodate the naphthyl rings. As a result, an angle of 17.9° between the two planes was observed rather than the typical ∼45° angle observed in the other **1-X** complexes (Figure S7). Additionally, the two naphthoxide ligands are bound in the same orientation on both faces of the complex in the solid state, with a 16.9° angle between the two planes of the naphthyl rings (Figure S8). Despite the steric crowding, the ^{1}H NMR spectrum exhibits a single peak for the $-SiMe_3$ groups at room temperature.

Attempts to form other **1-X** derivatives were generally unsuccessful (Scheme 1). Reaction of either **1-Cl** or **1-Br** with $[^nBu_4N]CN$ led to reduction to the corresponding uranium(IV)−monohalide product (Scheme 1b). This is in contrast to cyclometalated uranium(IV) derivatives of the tris(amido) framework, which were shown to readily undergo substitution with cyanide ligands, from uranium−iodide precursors.[26] Similarly, treating **1-F** with Me_3SiCN led to no reaction (Scheme 1c), despite the utility of this reagent in forming other uranium−cyanide complexes through the favorable elimination of Me_3SiF.[27] The inherent difficulty in installing the cyanide ligand in the **1-X** framework implies that it is thermodynamically unfavorable. Reaction of **1-Cl** with alkylsodium reagents such as $NaCH_2Ph$ and $NaCH_2SiMe_3$ at −21 °C, conditions known to be favorable for the formation of uranium−alkyl

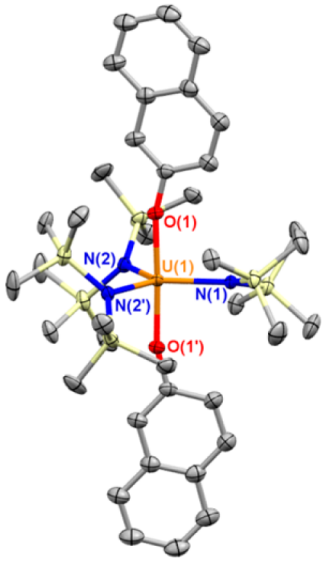

Figure 1. Thermal ellipsoid plot of **1-ONap** at 30% probability. Hydrogen atoms are omitted for clarity. Bond lengths (Å) and angles (deg): U(1)−O(1) 2.102(4), U(1)−N(1) 2.243(7), U(1)−N(2) 2.212(5), O(1)−U(1)−O(1′) 177.7(2).

complexes, led to immediate reduction to uranium(IV) (Scheme 1d), typically forming a mixture of the mono- and bis-metalacyclic products $U^{IV}(CH_2SiMe_2NSiMe_3)[N(SiMe_3)_2]_2$ and $[Na(THF)_x][U^{IV}(CH_2SiMe_2NSiMe_3)_2[N(SiMe_3)_2]]$,[28,29] as judged by ^{1}H NMR spectroscopy. The use of milder alkylating reagents such as MeMgBr or $(PhCH_2)_2Zn$ led to no reaction with **1-Cl**. Attempts to react **1-Cl** or **1-Br** with 2 equiv of NaCCPh in THF to form the corresponding uranium(V)−acetylide product also led to no reaction (Scheme 1e).

$U^VOX[N(SiMe_3)_2]_3^-$ Complexes (2-X). Complexes of the formula $UOX[N(SiMe_3)_2]_3^-$ (**2-X**) were synthesized through several routes. Initially, direct -ate complex formation was considered. For example, addition of NaN_3 to $U^VO[N(SiMe_3)_2]_3$ in THF led to a gradual color change from red to yellow-green. Analysis of the ^{1}H NMR spectrum showed a shift and desymmetrization of the $-SiMe_3$ resonances, with two resonances in a 1:1 ratio at −1.3 and −1.9 ppm, compared to the single resonance exhibited in the parent $U^VO[N(SiMe_3)_2]_3$ complex at −0.2 ppm.[30] The observed desymmetrization is analogous to that noted previously in **1-FCl**.[10] Crystallization from a THF solution layered with hexanes at −21 °C produced yellow-green crystals that underwent facile desolvation, significantly hindering quality X-ray diffraction data. Nevertheless, connectivity was established in the structure of $[Na(THF)_6][UO(N_3)[N(SiMe_3)_2]_3]$ (**2-N_3**), confirming that the -ate complex formation reaction was occurring (Supporting Information, Figure S10). In the solid state, **2-N_3** was quite unstable, decomposing to an unidentified insoluble colorless material within 1 d at −21 °C.

Use of a noncoordinating cation enabled the successful synthesis of the **2-X** complexes. The cyanide complex was accessible through reaction of $[Et_4N]CN$ with $U^VO[N(SiMe_3)_2]_3$ (Scheme 2), generating $[Et_4N][UO(CN)[N(SiMe_3)_2]_3]$ (**2-CN**) as a stable yellow-green product in 71% yield following recrystallization from Et_2O at −21 °C. Crystals of **2-CN** were quite robust, allowing X-ray diffraction (Figure 2). The U−CN bond length was 2.491(7) Å, shorter than that of the other known uranium(V) cyanide complexes $[^nBu_4N]_2[Cp^*_2U(CN)_5]$ (Cp = cyclopentadienyl) at 2.548(7) and $[Na(18\text{-crown-}6)][U(CN)[\kappa^2\text{-}OCH(=CH_2)SiMe_2N(SiMe_3)]_2[N(SiMe_3)_2]]$ at 2.565(7) Å.[26,31]

dx.doi.org/10.1021/ic500833s | Inorg. Chem. 2014, 53, 6944−6953

Scheme 2. Synthesis of 2-CN

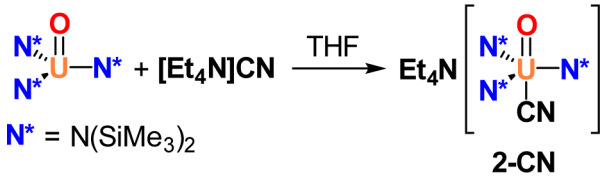

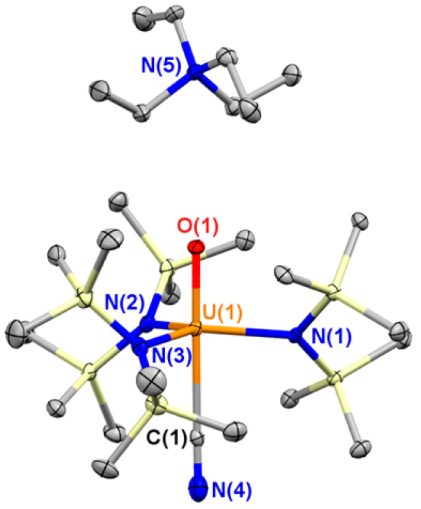

Figure 2. Thermal ellipsoid plot of **2-CN** at 30% probability. Hydrogen atoms are omitted for clarity. Bond lengths (Å) and angles (deg): U(1)–O(1) 1.847(4), U(1)–C(1) 2.491(7), U(1)–N(1) 2.273(5), U(1)–N(2) 2.246(5), U(1)–N(3) 2.283(4), C(1)–U(1)–O(1) 179.29(19).

The short U–CN bond length is attributed to the ITI stabilization imparted by the oxo ligand.

Attempts to form an acetylide linkage through addition of either NaCCPh or CuCCPh to $U^{V}O[N(SiMe_3)_2]_3$ led to no reaction, surprising given the high stability of our reported U(VI) product $UO(CCPh)[N(SiMe_3)_2]_3$.[12] However, treatment of $UO(CCPh)[N(SiMe_3)_2]_3$ with a reductant such as $NaCH_2Ph$ led to clean formation of $Na(THF)_6[UO(CCPh)-[N(SiMe_3)_2]_3]$ as judged by ^{1}H NMR spectroscopy, where the oxidation product bibenzyl was conveniently separated (Scheme 3). As observed in **2-N$_3$**, the Na-ate complex was

Scheme 3. Synthesis of 2-CCPh

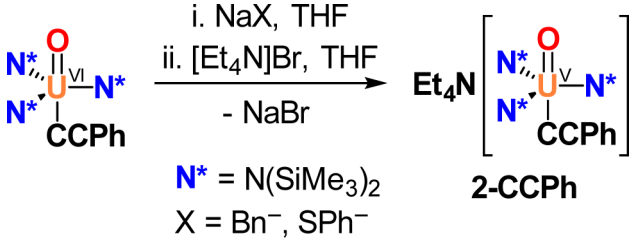

quite unstable, preventing further characterization due to decomposition even at low temperature. Subsequent addition of $[Et_4N]Br$ provided the much more stable $[Et_4N][UO-(CCPh)[N(SiMe_3)_2]_3]$ (**2-CCPh**). Production of **2-CCPh** was also possible through use of NaSPh as a reductant, though a side reaction to produce $U^{V}O[N(SiMe_3)_2]_3$ limited the utility of this route (Supporting Information, Figure S4).

The ^{1}H NMR spectra of the **2-X** complexes all displayed two resonances for the trimethylsilyl groups at room temperature, indicative of hindered rotation about the U–N bonds restricting the trimethylsilyl groups to chemically inequivalent environments. Similar behavior was noted in some of the related $U^{VI}OX[N(SiMe_3)_2]_3$ complexes (X = F, Cl, Me).[11,12] While some variability in the chemical shift of the **2-X** complexes was noted, in every case the two resonances were centered around −1.6 ppm at room temperature, similar to each case of the **1-X** complexes.[10] The independence of the ^{1}H chemical shift on axial substitution differs from complexes of the formulas $(CpMe_5)_2U(=N\text{-}2,6\text{-}^{i}Pr\text{-}C_6H_3)(X)$ (X = OTf^-, I^-, Br^-, Cl^-, SPh^-, $CCPh^-$, F^-, Me^-, OPh^-, $NCPh_2^-$), where a strong correlation between the donating ability of the X-ligand and the chemical shift of the C_5Me_5 ligands in the ^{1}H NMR spectra was observed, over a greater than 4 ppm range.[32]

Near-IR Spectroscopy. The electronic structures of the **1-X** and **2-X** complexes were probed using electronic absorption spectroscopy. The ^{2}F electronic state that arises from the $5f^1$ uranium(V) ion is perturbed by both spin–orbit coupling and ligand field splitting. As the spin–orbit coupling term is typically larger than the ligand field splitting, two sets of Stark sublevels comprising the $m_J = \pm 5/2$ (lower energy) and $m_J = \pm 7/2$ states are separated by ~7000 cm^{-1} ($\Delta E_{SOC} = 7/2\ \xi$; $\xi \approx 2000$ cm^{-1}).[14] As a result, four electronic transitions are expected in the near-IR (NIR) region. Given that the local symmetry at the uranium ion is maintained in the various complexes and that the spin–orbit coupling parameter ξ is known to be essentially independent of the ligand set for other uranium(V) complexes, the energy of the observed transitions can be used as a relative metric for the ligand field splitting parameters between the different complexes.

The **1-X** complexes all displayed four primary absorption bands of varying intensity in the NIR spectra between 7000 and 14 000 cm^{-1} (Figure 3). Some spectral broadening and shoulder features are noted in some of the peaks. Interestingly, the energy difference between the shoulder features and the primary absorptions in each case matches well with the axial uranium–ligand stretching frequencies, confirmed through density functional theory (DFT) calculations (Table 1). Only the asymmetric F–U–F stretch in **1-F** was in an experimentally accessible range, which was previously noted at 511 cm^{-1},[10] in good agreement with the energy difference observed in the NIR spectrum of **1-F** at 510 cm^{-1}. These features therefore are assigned as vibronic progressions along the primary molecular axis. Vibronic transitions are known in octahedral uranium(V) complexes, where 5f–5f transition intensity is much lower,[14,15,33] and have also been observed in the low-temperature NIR spectra of complexes of the formula $(C_5Me_5)_2U(=N\text{-}2,6\text{-}^{i}Pr_2\text{-}C_6H_3)(X)$ (X = F^-, Cl^-, Br^-, I^-).[32] Since the axial metal–ligand vibrations of the **1-X** complexes are strongly associated with the highest energy f–f transition, these bands are assigned as transitions into the $5f_z^3$ σ^* orbital. Notably, significant vibronic intensity is observed in a lower energy band in **1-NCS**. This is attributed to greater mixing of the f orbitals in **1-NCS**, indicating that the thiocyanate ligand does not impart a strong primary axis.

The NIR spectra of the **2-X** complexes were comparatively simpler and more interpretable (Figure 4). Each of the derivatives exhibited four primary excitations as expected, of similar intensity. The f–f transitions were observed at lower intensity relative to the **1-X** complexes. Similar NIR spectra have been reported for other uranium(V) complexes bearing a single oxo ligand.[30,34,35] In the NIR spectrum of **2-CN**, the

dx.doi.org/10.1021/ic500833s | Inorg. Chem. 2014, 53, 6944–6953

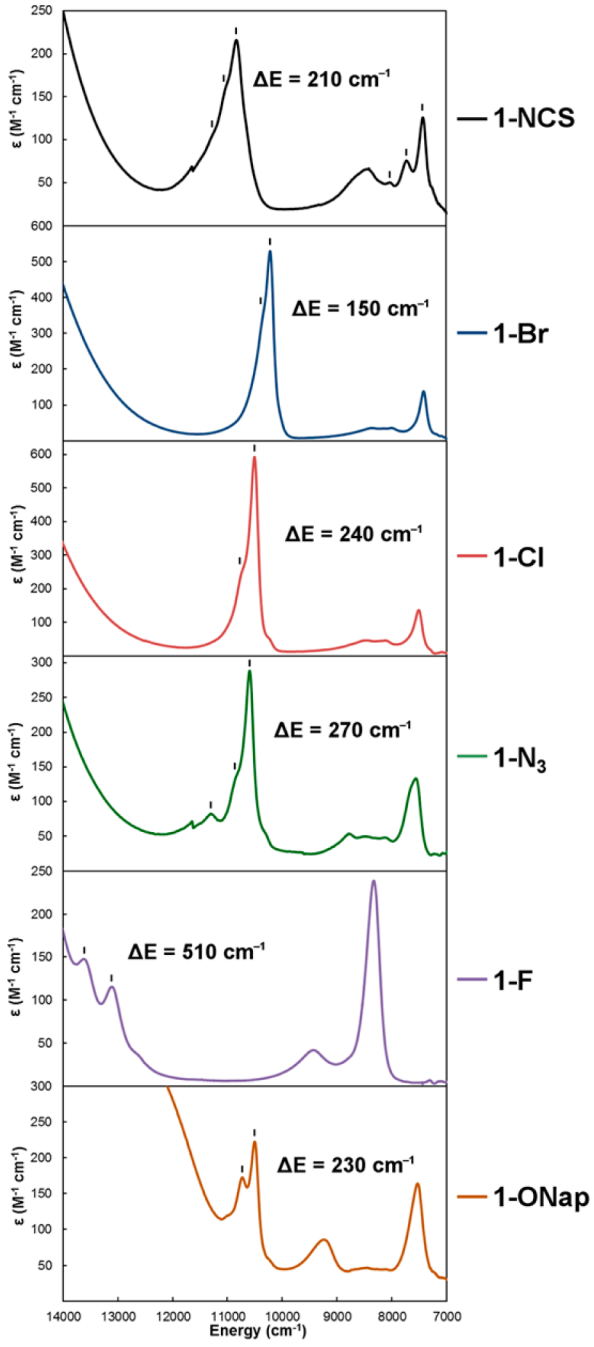

Figure 3. Near-IR spectra of the **1-X** complexes in toluene. Peaks assigned as vibronically resolved transitions are labeled with vertical black lines, with the energy splitting indicated. The spectrum of **1-Cl** was previously reported.[10]

Table 1. Comparison of Observed Vibronic Transitions and Calculated Axial Asymmetric X–U–X Stretching Frequencies in the 1-X Complexes

	ΔE (NIR) (cm^{-1})	calculated ν_{X-U-X} (cm^{-1})
1-NCS	210	225
1-Br	150	187
1-Cl	240	255
1-N_3	270	294
1-F	510	518
1-ONap	230	238

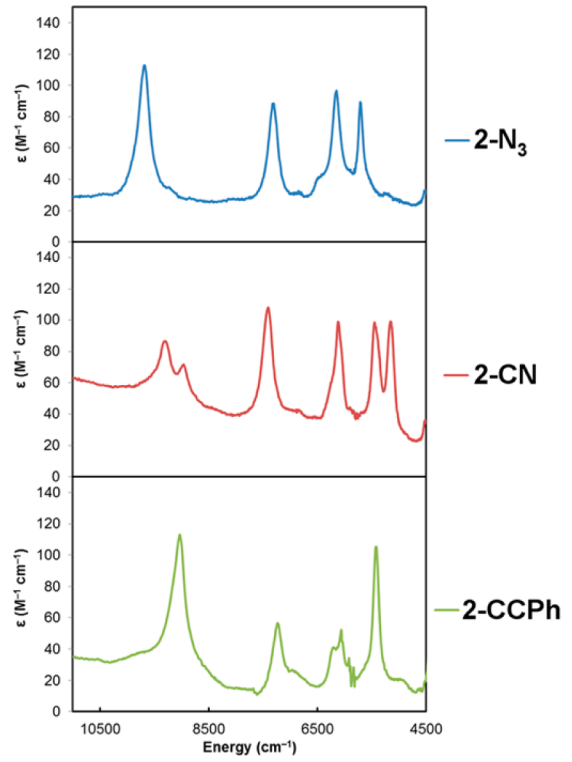

Figure 4. Near-IR spectra of **2-CN**, **2-N_3**, and **2-CCPh** in CH_2Cl_2. The peak at 6127 cm^{-1} in the spectrum of **2-CCPh** is partially occluded by solvent overtones.

highest and lowest energy f–f transitions exhibited splitting similar to the spectrum of **1-NCS**.

Electrochemistry. Electrochemical measurements were carried out on CH_2Cl_2 solutions of the **1-X** complexes in an effort to assess their relative stability (Figure 5, Table 2). Among the **1-X** complexes, reversible waves were observed in the cyclic voltammograms (CVs) at $E_{1/2} \approx +0.9$ V versus a ferrocene/ferrocenium internal standard. These waves were assigned to a U^{VI}/U^{V} redox process. The reduction feature of the U^{VI}/U^{V} wave became more reversible at faster scan rates, indicating that the U^{VI} product is unstable under the conditions of the experiment. The electrochemical accessibility of the U(VI/V) couple did not vary significantly between the dihalide complexes, but the potential was ~100 mV greater in the pseudohalide complex **1-NCS** and ~150 mV lower in **1-ONap**. A second reversible feature was observed for each complex, assigned as a U^{V}/U^{IV} redox process. The potential of this process was more sensitive to the identity of the axial ligand (Table 1). The potential was smallest for the difluoride complex **1-F** and largest for the dithiocyanate complex **1-NCS**. These data suggest that the donor strength of the axial ligand increases in the order $NCS^- < Br^- < Cl^- < N_3^- < F^- \approx ONap^-$.

Electrochemical measurements were also carried out on the **2-X** complexes for comparison. Both the $U^{VI/V}$ and $U^{V/IV}$ couple were significantly shifted relative to the **1-X** complexes. In the case of **2-CN**, the $U^{VI/V}$ couple appeared as a reversible feature centered at −0.23 V, and the $U^{V/IV}$ couple was irreversible, with a large wave separation of ~1 V (Figure 6). Use of differential pulse voltammetry (DPV) allowed determination of the reduction potential, at −1.96 V. The large deviation of the E_{pa} wave from the potential obtained by DPV suggests a large kinetic barrier to oxidation of the electrochemically formed uranium(IV) species. The CV of

dx.doi.org/10.1021/ic500833s | Inorg. Chem. 2014, 53, 6944–6953

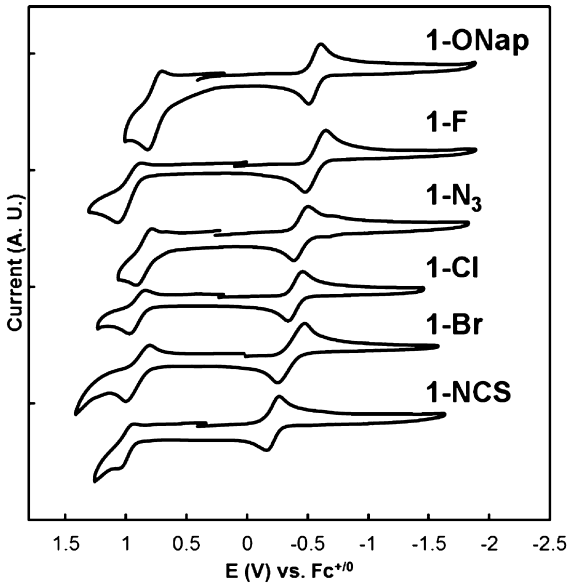

Figure 5. Cyclic voltammograms of the **1-X** complexes in CH_2Cl_2 with 0.1 M [$^nBu_4N$][PF_6] supporting electrolyte. The electrochemical data for **1-Cl** was previously reported.[10]

Table 2. Electrochemical Data for the 1-X and 2-X Complexes

	$E_{1/2}$(eV)	
	$U^{VI/V}$	$U^{V/IV}$
1-NCS	1.00	−0.21
1-Br	0.89	−0.37
1-Cl	0.91	−0.40
1-N_3	0.85	−0.45
1-F	0.98	−0.57
1-Onap	0.76	−0.56
2-CN	−0.23	−1.96
2-N_3	−0.48	−2.08
2-CCPh	−0.59	

freshly prepared **2-N_3** (Supporting Information, Figure S34) closely resembled that of **2-CN**, with both the reduction and oxidation couple shifted to more negative potentials, at −0.48 and −2.08 V, respectively. Again, a separation of the waves of the reduction feature of ∼1 V was observed, necessitating the determination of the $E_{1/2}$ with DPV. The CV of **2-CCPh** (Supporting Information, Figure S38) showed a reversible $U^{VI/V}$ couple at −0.59 V, in good agreement with the potential of −0.51 V that we previously measured for the uranium(VI) complex, $U^{VI}O(CCPh)[N(SiMe_3)_2]_3$.[12] The $U^{V/IV}$ reduction couple was not observed in either the CV or DPV measurements of **2-CCPh**, leading us to conclude that it must appear at a lower potential than could be measured under the experimental conditions.

Variable-Temperature ^{1}H NMR Data. We previously noted that at room temperature, **1-F** displayed a single resonance in the ^{1}H NMR spectrum, whereas **1-Br** displayed three well-separated peaks in a 1:1:1 ratio and **1-Cl** displayed three broad, partially overlapping peaks.[10] We attributed this behavior to the hindered rotation of the $-SiMe_3$ groups by the axial ligands, creating three distinct chemical environments. We therefore carried out variable-temperature (VT) ^{1}H NMR measurements on the halide derivatives of the **1-X** complexes to determine the barrier to rotation (Figure 7). Decoalescence of

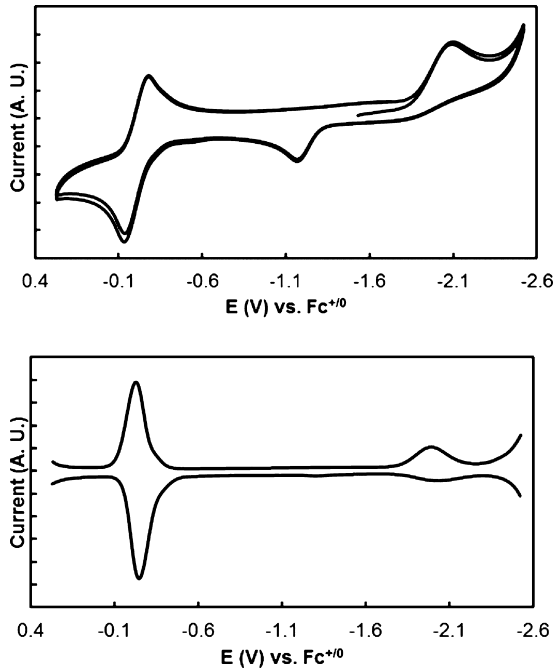

Figure 6. Cyclic voltammogram (top) and differential pulse voltammogram (bottom) of **2-CN** in CH_2Cl_2, with 0.1 M [$^nBu_4N$]-[PF_6] supporting electrolyte.

the single resonance into three resonances in a 1:1:1 ratio was observed in all of the complexes, though one resonance was too broad to precisely identify in **1-F**. The silylamide rotational barriers were found to scale directly with the ionic radii of the axial ligands (Figure 8), by a factor of 6.96 kcal mol^{-1} $Å^{-1}$. An intercept of 0.04 kcal/mol was obtained, close to the idealized value of zero. We similarly determined the coalescence temperature and corresponding barrier to rotation in **1-N_3**. Using the empirical relation established between the barrier to rotation and ionic radius in the dihalide congeners, we calculated an effective ionic radius for the azide ion of 1.58 Å, precisely the value obtained through analysis of the structure of KN_3,[36] further supporting the validity of this analysis. The room-temperature ^{1}H NMR spectra showed little variation in the $-SiMe_3$ resonances (around −1.5 ppm) with no correlation with axial donor strength (Supporting Information, Figure S7), so the correlation between the ionic radius and the barrier to rotation is useful for characterizing the ^{1}H NMR spectra of related complexes.

Electronic Structure Calculations. In our previous work, we observed features of the ITI in the series of $U^{VI}OX[N(SiMe_3)_2]_3$ complexes, which allowed the determination of an ITI ligand series.[12] Additionally, we previously noted features of the ITI in the electronic structure of **1-Cl**, including $5f_z^3$−$6p_z$ mixing.[10] It was therefore of interest whether subtle variations in ITI stabilization would extend to the pentavalent **1-X** derivatives. DFT calculations on all of the **1-X** complexes gave good agreement with the experimental bond metrics (Table 3). The naphthyl groups in the **1-ONap** complex were truncated to phenyl groups for the sake of computational simplicity (**1-OPh**). Notably, the near coplanarity of the aryl rings and slight distortion of the U−O−C bonds from linearity was reproduced computationally, even with the truncation in **1-OPh**.

Examination of the molecular orbitals involved in axial bonding in **1-OPh** showed mutual π donation of the aryloxides into the unfilled $5f_{yz}^2$ orbital in the highest occupied molecular

dx.doi.org/10.1021/ic500833s | Inorg. Chem. 2014, 53, 6944−6953

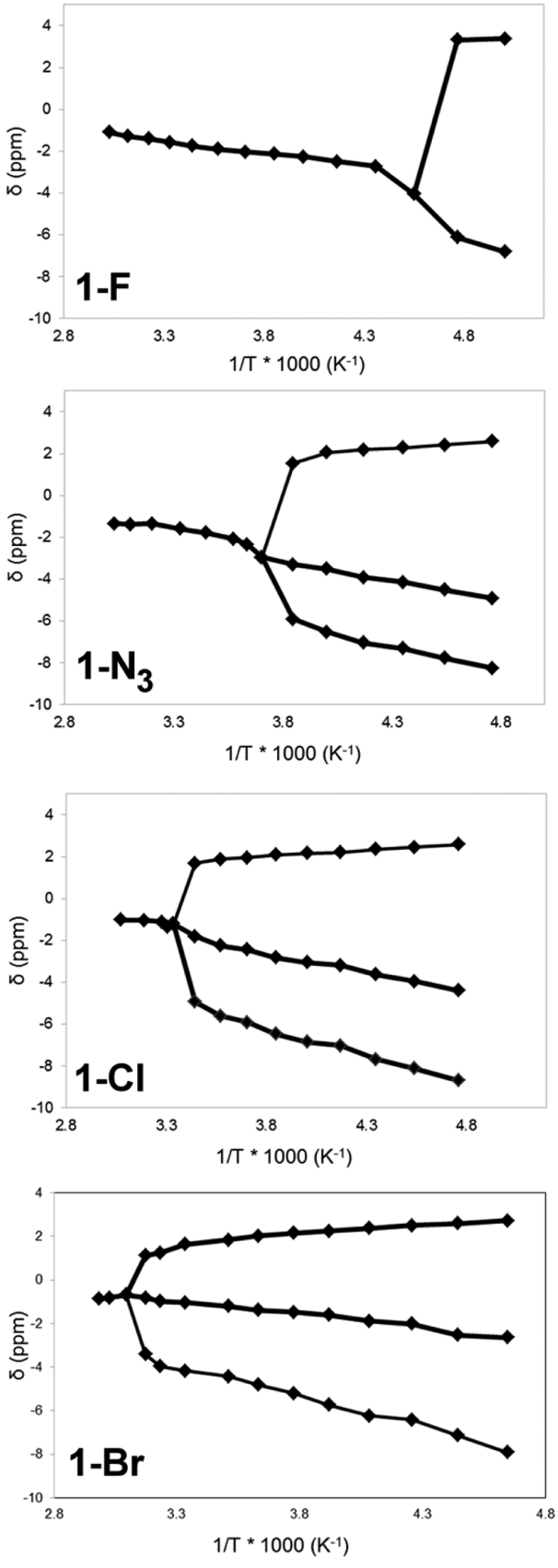

Figure 7. Top to bottom: VT ^{1}H NMR data for **1-F**, **1-N$_3$**, **1-Cl**, and **1-Br** collected in C_7D_8. Following decoalescence, the third resonance was too broad to accurately determine for **1-F**.

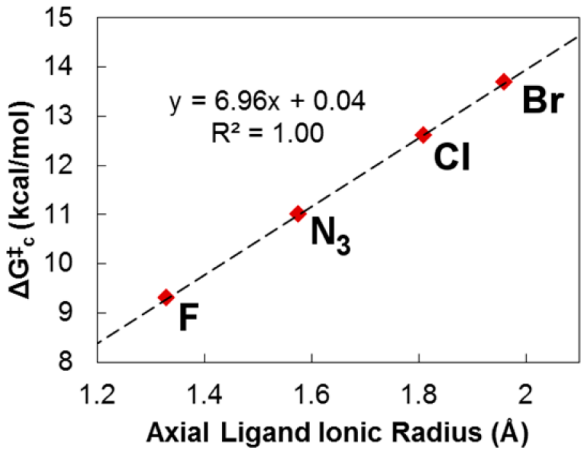

Figure 8. Correlation between the barrier to rotation of the trimethylsilyl groups in the **1-X** complexes with the ionic radius of the axial ligand.

Table 3. Physical and Calculated Data for the 1-X Complexes

	U−X bond length (Å)		U−N bond length (Å)		U−N Mayer bond order
	exp.	calc.	exp.	calc.	
1-CN		2.488		2.168	1.589
1-NCS[a]	2.316(9)	2.295	2.154(8)	2.191	1.554
1-Br[a]	2.745(1)	2.773	2.164(4)	2.189	1.513
1-Cl[a]	2.575(1)	2.627	2.166(1)	2.192	1.459
1-N$_3$[b]	2.226(3)	2.229	2.167(3)	2.212	1.503
1-F[a]	2.066(2)	2.067	2.189(2)	2.220	1.402
1-ONap/1-OPh	2.102(4)	2.111	2.222(5)	2.262	1.379

[a]Experimental data from reference 10. [b]Experimental data from reference 25.

orbital (HOMO)−18, with the corresponding π^* interaction present as the lowest unoccupied molecular orbital (LUMO)+4 (Figure 9). Analysis of the atomic orbital (AO) composition of these molecular orbitals (MOs) showed 7% uranium 5f AO character in the bonding MO and 85% uranium 5f AO character in the antibonding MO, with negligible 6d character. Similar mutual π-bonding interactions are observed in complexes of uranyl.[2] The requisite symmetry of this interaction is likely the basis for the preference for coplanarity of aryloxide ligands.

Within the series of **1-X** complexes, evidence for cis-destabilization was considered as an indirect metric for ITI stabilization. At the extremes of the series of donor strengths established by the electrochemical data, namely, at complexes **1-ONap** and **1-NCS**, the U−N bond lengths differed experimentally by ∼0.068 Å and computationally by 0.071 Å. However, minor variations in the bond lengths among the intermediate complexes were too close to reliably differentiate. A more significant trend was observed in the Mayer bond order (MBO) of the equatorial U−N bonds, which vary following the order established from the potential of the $U^{V/IV}$ couple, indicating that as the U−N bond order increases, the 5+ oxidation state becomes less stable relative to the 4+ state. This result is perhaps counterintuitive, as a larger MBO for an identical ligand in two complexes is expected to increase the electron density at the metal center, which should lead to a decrease in the reduction potential rather than the observed increase. The axial ligand therefore plays a significant role not only in stabilizing the high oxidation state but also in

dx.doi.org/10.1021/ic500833s | Inorg. Chem. 2014, 53, 6944−6953

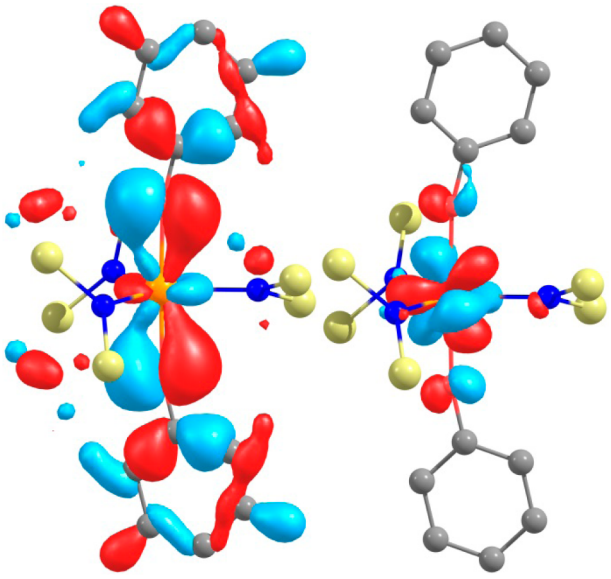

Figure 9. Primary axial π-bonding (HOMO−18, left) and π^*-antibonding (LUMO+4, right) molecular orbitals in **2-OPh**. Hydrogen atoms and methyl groups are omitted for clarity.

modulating the equatorial metal−ligand bonding, consistent with the cis-destabilization that arises from the ITI.[9,12]

Extrapolating the observed trend to the theoretical **1-CN** gave an indication of the instability of this complex, as the equatorial bonding analysis showed that the U−N MBO was even greater than that of **1-NCS**, suggesting that the cyanide ligand is poor at stabilizing the 5+ oxidation state in this system. As was previously calculated for the theoretical $U^{VI}O(CN)[N(SiMe_3)_2]_3$ complex,[12] cyanide appears to be a poor axial ligand for high-valent uranium.[37]

Analysis of the equatorial σ bonding in the **1-X** complexes showed significant variation in the contribution of uranium AO character (Table 4). Greater contribution of uranium AO character toward bonding is indicative of a more covalent bond. Notably, the complexes with the strongest axial donors, as judged by stabilization of the 5+ oxidation state inferred from the reduction potential, exhibited the least covalent equatorial bonding. However, there was no correlation between equatorial covalency and uranium natural charge (q_U). Variations in uranium natural charge were attributed to differences in electronegativity of the axial donor ligands. Therefore, stronger axial donors destabilize cis-coordination through a reduction in covalent interaction, a feature of the ITI that has been previously observed.[9,12]

Table 4. DFT Calculated Metrics of 1-X Complexes

	%U in U−N_{eq} NBOs	q_U	U($6p_z$) depopulation
1-CN	16.56	1.31	−0.102
1-NCS	16.16	1.56	−0.096
1-Br	15.29	0.87	−0.099
1-Cl	14.41	1.00	−0.108
1-N_3	16.27	1.41	−0.101
1-F	12.20	1.80	−0.094
1-ONap	7.03	1.74	−0.099

Depletion of semicore 6p AO character at the uranium center, a feature of the ITI,[1,2,38] was also investigated. Mixing of the $6p_z$ orbital with the $5f_z^3$ orbital in an axial σ-bonding MO was previously noted in the electronic structure of **1-Cl**. Analysis of the uranium AO parentages in the optimized **1-X** complexes showed depopulation of the $6p_z$ orbital, of approximately −0.10 α-spin electrons, with little variation between the complexes (Table 4). The magnitude of the depopulation was smaller than it was in related uranium(VI) complexes, which showed a range of $6p_z$ depopulation varying between −0.14 and −0.18 α-spin electrons.[11]

Comparison of the LUMO through LUMO+5 of the **1-X** halide and pseudohalide complexes showed that progressing to the weaker axial donors led to some stabilization of the σ^* and π^* orbitals, and finally substantial mixing of multiple f orbitals in **1-NCS** (Supporting Information, Figure S47). The poor ligand NCS^- did not impose a strong primary axis along the X−U−X vector, leading to mixing of the antibonding MOs. A notable exception to this trend was the complex **1-Cl**, where the LUMO+5 of primarily $5f_z^3$ character was destabilized almost to the same extent as that of **1-F**; however, the relative energies of the π^* MOs, namely, the LUMO+3 and LUMO+4 in **1-F** and the LUMO+2 and LUMO+3 in **1-Cl**, showed that the fluoride ligand is a stronger π-donor. The ability for fluoride to act as a π-donor to high-valent uranium has been noted previously.[37]

An illustration of the effect of the axial ligand in the **1-X** complexes was obtained from the density of states (DOS) plots. The partial and total DOS plots quantified the relative orbital contribution of the uranium, equatorial amide ligands, and axial ligands to the total MO character at a particular energy level. A high degree of uranium AO character energetically matched to a linear combination of atomic orbitals (LCAO) originating from a set of ligands is a prerequisite feature for a bonding interaction. In the DOS plots of **1-OPh** (Supporting Information, Figure S48), **1-F** (Supporting Information, Figure S49), **1-Cl** (Supporting Information, Figure S50), **1-Br** (Supporting Information, Figure S51), and to a lesser extent **1-N_3** (Supporting Information, Figure S52) the appearance of uranium AO character was well-matched to the AO character originating from the axial ligands. In contrast, in the **1-NCS** (Supporting Information, Figure S53) and **1-CN** (Supporting Information, Figure S54) DOS plots, it is evident that uranium AO character was more strongly correlated to AO character arising from the equatorial amide ligands. An increase in equatorial uranium−ligand bond covalency with weaker axial donors was previously identified in uranium(VI) complexes.[9,12]

EPR Spectroscopy. The EPR spectra of the **1-X** complexes were collected at 5 K with an X-band spectrometer as toluene glasses (Figure 10 and Supporting Information, Figures S42−S46). All of the spectra exhibited a sharp signal centered at g = ∼2.2 and an extremely broad feature centered at g = ∼0.7, attributed to $g_\parallel$ and $g_\perp$, respectively. The presence of an EPR signal indicated that the ground state was the μ = 1/2 state in every complex, as the μ = 3/2 state is not EPR-active.[39,40] In a recent survey of EPR data by Liddle and co-workers,[41] a range of values of $g_\parallel$ of 1.1−2.2 and $g_\perp$ of 0.7−2.4 was established for anisotropic uranium(V) complexes.[14,20,34,42−46] The g values of the **1-X** complexes are therefore at the extrema of these ranges, indicating a high degree of anisotropy.

We recently reported the spectrum of **1-Cl**, in which no obvious hyperfine coupling was noted, suggesting that the single unpaired electron resides solely on the uranium ion.[10] Similar spectra were reported by Hayton, Lukens, and co-workers for the compounds $U^VO[N(SiMe_3)_2]_3$ and $[Ph_3PCH_3][U^VO(CH_2SiMe_2NSiMe_3)[N(SiMe_3)_2]_2]$.[30,35] In

dx.doi.org/10.1021/ic500833s | Inorg. Chem. 2014, 53, 6944−6953

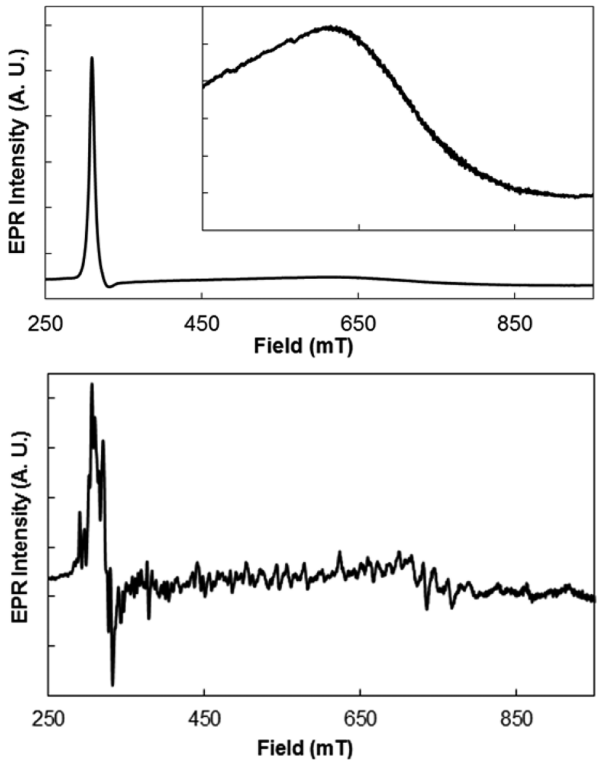

Figure 10. EPR spectrum of **1-Cl** (top) and **1-N_3** (bottom) at 5 K. The region between 450 and 950 mT in the spectrum of **1-Cl** is enhanced in the inset. The EPR spectrum of **1-Cl** was previously reported[10] and is shown for comparison.

contrast, the EPR spectra of **1-N_3** (Figure 10, bottom) and **1-NCS** (Supporting Information, Figure S46) exhibited extensive hyperfine coupling. In the case of **1-N_3**, assuming that the hyperfine coupling terms are equivalent between the chemically equivalent nitrogen atoms of the two azide ligands, and that each of the three nitrogen atoms exhibits a different coupling constant, a pentet of pentet of pentets would be expected, totaling 125 peaks.

The excess α-spin density in each of the DFT-calculated **1-X** complexes was investigated to corroborate the results of the EPR experiments (Supporting Information, Figures S55−S59). All of the complexes showed isolation of the α-spin to the uranium center, with minor excess β-spin density on the atoms directly bound to the uranium center due to spin contamination.[47] The absence of α-spin density on the azide ligands in **1-N_3** was surprising given the extensive coupling of the unpaired electron inferred from the EPR experiment. The presence of hyperfine coupling in the EPR spectrum may indicate that the electronic structure is more complicated than that described by the DFT method.[48]

CONCLUSIONS

Characterization of a family of trigonal bipyramidal uranium complexes provided a glimpse into the role of the ITI in pentavalent uranium. These complexes exhibit spectroscopic features consistent with a dominant axial symmetry, including vibronic coupling, and axial EPR signals with hyperfine coupling, both along the primary molecular axis. Experimental determination of the axial ligand donor strength revealed a trend, $NCS^- < Br^- < Cl^- < N_3^- < F^- < ONap^-$, that was correlated to the calculated ITI stabilization imparted by each ligand. The presence of the strong ITI oxo ligand allowed the synthesis of uranium(V) cyanide and phenylacetylide bonds that were otherwise inaccessible in our hands. New strategies using the ITI to stabilize reactive uranium−ligand bonds and a more detailed crystal field analysis of these complexes are under consideration.

EXPERIMENTAL SECTION

General Methods. All reactions and manipulations were performed under an inert atmosphere (N_2) using standard Schlenk techniques or in a Vacuum Atmospheres, Inc. Nexus II drybox equipped with a molecular sieves 13X/Q5 Cu-0226S catalyst purifier system. Glassware was oven-dried overnight at 150 °C prior to use. ^{1}H NMR spectra were obtained on a Bruker DMX-300 Fourier transform NMR spectrometer at 300 MHz. Chemical shifts were recorded in units of parts per million downfield from residual proteo solvent peaks. VT NMR data were collected in toluene-d_8 using a BVT 2000 unit, and samples were checked for decomposition following data collection. Elemental analyses were performed at the University of California, Berkeley Microanalytical Facility using a PerkinElmer Series II 2400 CHNS analyzer. UV−vis−NIR data were collected on a Cary 5000 spectrometer in toluene in 1 mm path length air-free quartz cuvettes between 275 and 2500 nm. Background corrections were made using pure toluene to reduce vibrational overtones in the NIR region due to solvent. The IR spectra were obtained from 400−4000 cm^{-1} using a PerkinElmer 1600 series IR spectrometer. EPR spectra of samples frozen in toluene glass were collected on a Bruker Elexsys 500 spectrometer at X-band frequency (9.4 GHz), with the temperature set to 5 K with an Oxford Instrument ESR900 helium flow cryostat.

Materials. Tetrahydrofuran, Et_2O, CH_2Cl_2, hexanes, *n*-pentane, and toluene were purchased from Fisher Scientific. These solvents were sparged for 20 min with dry argon and dried using a commercial two-column solvent purification system comprising columns packed with Q5 reactant and neutral alumina, respectively (for hexanes and *n*-pentane), or two columns of neutral alumina (for THF, Et_2O, and CH_2Cl_2). All solvents were stored over 3 Å molecular sieves. Deuterated solvents were purchased from Cambridge Isotope Laboratories, Inc. and stored over potassium mirror overnight prior to use. Starting materials $U^{III}[N(SiMe_3)_2]_3$,[49] $UCl[N(SiMe_3)_2]_3$,[50] $UO[N(SiMe_3)_2]_3$,[30] $UF_2[N(SiMe_3)_2]_3$,[10] $UBr_2[N(SiMe_3)_2]_3$,[10] $U(N_3)_2[N(SiMe_3)_2]_3$,[10,25] $U(NCS)_2[N(SiMe_3)_2]_3$,[10] and $UO(CCPh)$-$[N(SiMe_3)_2]_3$[12] were prepared according to the reported procedures. NaN_3 (Strem) was dried at 100 °C under reduced pressure overnight prior to storage in the glovebox, and $[Et_4N]CN$ (Aldrich) and $[Et_4N]Br$ (Acros) were used as received.

Electrochemistry. Voltammetry experiments (CV) were performed using a CH Instruments 620D Electrochemical Analyzer/Workstation, and the data were processed using CHI software v9.24. All experiments were performed in a N_2 atmosphere drybox using electrochemical cells that consisted of a 4 mL vial, glassy carbon working electrode, a platinum wire counter electrode, and a silver wire plated with AgCl as a quasi-reference electrode. The working electrode surfaces were polished prior to each set of experiments. Potentials were reported versus ferrocene, which was added as an internal standard for calibration at the end of each run. Solutions employed during these studies were ∼3 mM in analyte and 100 mM in $[^nBu_4N][PF_6]$ in 2 mL of dichloromethane. All data were collected in a positive-feedback IR compensation mode.

X-ray Crystallography. X-ray intensity data were collected on a Bruker APEXII CCD area detector employing graphite-monochromated Mo Kα radiation (λ = 0.710 73 Å) at a temperature of 143(1) K. In all cases, rotation frames were integrated using SAINT,[51] producing a listing of unaveraged F^2 and $\sigma(F^2)$ values which were then passed to the SHELXTL[52] program package for further processing and structure solution. The intensity data were corrected for Lorentz and polarization effects and for absorption using TWINABS[53] or SADABS.[54] The structures were solved by direct methods (SHELXS-97).[55] Refinement was by full-matrix least-squares based on F^2 using SHELXL-97.[55] All reflections were used during

dx.doi.org/10.1021/ic500833s | Inorg. Chem. 2014, 53, 6944−6953

refinements. Non-hydrogen atoms were refined anisotropically, and hydrogen atoms were refined using a riding model.

Computational Details. All calculations were performed with Gaussian 09 Revision C.01,[56] with the B3LYP hybrid DFT method. Effective core potentials incorporating quasi-relativistic effects were applied to uranium, with a 60 electron core and the corresponding segmented natural orbital basis set.[57,58] Geometry optimizations were carried out in C_1 symmetry for all uranium complexes, as higher symmetry solutions were either higher in energy or were not successfully converged. All frequency calculations found no imaginary frequencies, confirming that the optimized structures were minima. Compositions of MOs and DOS plots were calculated using the AOMix program.[59,60]

Synthesis of U(ONap)$_2$[N(SiMe$_3$)$_2$]$_3$ (1-ONap). To a stirred, opaque solution of **1-Cl** (150 mg, 0.19 mmol) in THF, K(THF)$_{0.5}$-(2-naphthoxide) (124 mg, 0.57 mmol, 3.0 equiv) was added, resulting in a color change to pale orange. After 30 min, $CuBr_2$ (212 mg, 0.95 mmol, 5.0 equiv) was added, resulting in a color change to red-black and then to green-black. After 15 min, the volatiles were removed under reduced pressure, and the black residue was extracted with hexanes and filtered over Celite suspended in a glass pipet; the volatiles were removed under reduced pressure. The black residue was dissolved in minimal Et_2O and stored at −21 °C to yield **1-ONap** as black crystals. Crystals suitable for X-ray diffraction were obtained from a concentrated hexanes solution stored at −21 °C. Yield: 111 mg, 0.11 mmol, 58%. ^{1}H NMR (benzene-d_6): 14.23 (2H, fwhm = 42 Hz), 12.75 (2H, fwhm = 14 Hz), 12.18 (2H, fwhm = 39 Hz), 9.97 (2H, fwhm = 15 Hz), 8.94 (2H, fwhm = 18 Hz), 8.70 (2H, fwhm = 15 Hz), 7.55 (2H, fwhm = 18 Hz), −1.92 (54H, fwhm = 39 Hz). Elemental analysis found (calculated) for $C_{38}H_{68}N_3O_2Si_6U{\cdot}0.5Et_2O$: C, 46.15 (46.08); H, 6.72 (7.06); N, 3.54 (4.03)%.

Synthesis of [Na(THF)$_n$][U^{V}O(N$_3$)[N(SiMe$_3$)$_2$]$_3$] (2-N$_3$). To a red-orange solution of UO[N(SiMe$_3$)$_2$]$_3$ (20 mg, 0.03 mmol) in 3 mL of THF, NaN_3 (18 mg, 0.28 mmol, 10.0 equiv) was added. The mixture was stirred for 1 h, over which time it slowly turned green-yellow. The mixture was filtered over Celite suspended in a glass pipet, concentrated, layered with hexanes, and stored at −21 °C to yield **2-N$_3$** as green-yellow plates. Drying samples of **2-N$_3$** produced an unstable yellow powder that decomposed overnight at −21 °C, precluding solid-state characterization including elemental analysis. ^{1}H NMR (4:1 benzene-d_6/pyridine-d_5): δ 3.60 (12H, fwhm = 24 Hz), 1.47 (12H, fwhm = 24 Hz), −1.33 (27H fwhm = 27 Hz), −1.88 (27H, fwhm = 27 Hz). FTIR (THF): 2101(s, ν_{azide}), 2084 (s, ν_{azide}).

Synthesis of [Et$_4$N][U^{V}O(CN)[N(SiMe$_3$)$_2$]$_3$] (2-CN). To a red-orange solution of UO[N(SiMe$_3$)$_2$]$_3$ (43 mg, 0.06 mmol) in 3 mL of THF, [Et$_4$N][CN] (9.1 mg, 0.06 mmol, 1.0 equiv) was added, resulting in an immediate color change to green-yellow. After it was stirred for 20 min, the reaction mixture was filtered through Celite suspended in a glass pipet, and the volatiles were removed under reduced pressure. The resulting green-yellow powder was rinsed with *n*-pentane to provide pure **2-CN**. Single crystals suitable for X-ray diffraction were obtained from recrystallization of a concentrated Et_2O solution stored at −21 °C. Yield: 37 mg, 0.04 mmol, 71%. ^{1}H NMR (pyridine-d_5): 3.85 (8H, fwhm = 21 Hz), 1.65 (8H, fwhm = 21 Hz), −1.14 (27H, fwhm = 36 Hz), −1.92 (27H, fwhm = 33 Hz). IR (KBr): 3379 (m), 2923 (s), 2852 (m), 2058 (w, $\nu_{C\equiv N}$), 1540 (m), 1456 (m), 1384 (s), 1344 (m), 1181 (w), 1083 (w), 922 (s), 845 (s), 775 (m) 665 (m, ν_{U-N}), 612 (m, ν_{U-N}). Elemental analysis found (calculated) for $C_{35}H_{90}N_5OSi_6U$: C, 36.68 (36.38); H, 8.30 (8.37); N, 7.51 (7.86)%.

Synthesis of [Et$_4$N][UO(CCPh)[N(SiMe$_3$)$_2$]$_3$] (2-CCPh). To a dark green-brown solution of UO(CCPh)[N(SiMe$_3$)$_2$]$_3$ (70 mg, 0.08 mmol) in THF, a THF solution of $NaCH_2Ph$ (10 mg, 0.09 mmol, 1.10 equiv) was added, resulting in an immediate color change to light brown-orange. After the mixture was stirred for 10 min, [Et$_4$N]Br (18 mg, 0.09 mmol, 1.10 equiv) was added, resulting in a slow color change to yellow-brown. After it was stirred for 1.5 h, the cloudy mixture was filtered through Celite suspended in a glass pipet, and the volatiles were removed under reduced pressure. The resulting brown residue was dissolved in Et_2O, filtered through Celite suspended in a glass pipet, concentrated, and stored at −21 °C to afford **2-CCPh** as a tan crystalline solid, which was rinsed with *n*-pentane and dried under reduced pressure. Yield: 54 mg, 0.06 mmol, 66%. ^{1}H NMR (pyridine-d_5): 13.12 (2H, fwhm = 15 Hz, *o*-H), 9.52 (2H, fwhm = 15 Hz, *m*-H), 9.07 (1H, fwhm = 15 Hz, *p*-H), 3.43 (8H, fwhm = 24 Hz, NCH_2CH_3), 1.32 (8H, fwhm = 16 Hz, NCH_2CH_3), −1.35 (27H, fwhm = 21 Hz), −2.03 (27H, fwhm = 12 Hz). IR (KBr): 3383 (m), 2921 (s), 2852 (m), 1537 (s), 1455 (m), 1384 (vs), 1253 (m), 1181 (m), 1084 (m), 890 (s), 775 (m). 691 (w), 667 (m, ν_{U-N}), 612 (m, ν_{U-N}). Elemental analysis found (calculated) for $C_{34}H_{79}N_4OSi_6U$: C, 42.16 (42.25); H, 8.36 (8.24); N, 5.93 (5.80)%.

■ ASSOCIATED CONTENT

Ⓢ Supporting Information

^{1}H NMR spectra, crystallographic data (CIFs), electrochemical data, EPR spectra, and computational data. This material is available free of charge via the Internet at http://pubs.acs.org.

■ AUTHOR INFORMATION

Corresponding Author

*E-mail: schelter@sas.upenn.edu.

Notes

The authors declare no competing financial interest.

■ ACKNOWLEDGMENTS

We acknowledge the Research Corporation for Science Advancement (Cottrell Scholar Award to E.J.S.), the National Science Foundation (CHE-1362854) and the University of Pennsylvania for financial support. We thank the U.S. National Science Foundation for support of the X-ray diffractometer used in this work (CHE-0840438). This work used the Extreme Science and Engineering Discovery Environment (XSEDE), which is supported by U.S. National Science Foundation Grant No. OCI-1053575. We thank Prof. C. R. Graves (Albright College) for helpful discussion.

■ REFERENCES

(1) O'Grady, E.; Kaltsoyannis, N. *J. Chem. Soc., Dalton Trans.* **2002**, 1233−1239.

(2) Denning, R. G. *J. Phys. Chem. A* **2007**, *111*, 4125−4143.

(3) King, D. M.; Tuna, F.; McInnes, E. J.; McMaster, J.; Lewis, W.; Blake, A. J.; Liddle, S. T. *Nat. Chem.* **2013**, *5*, 482−488.

(4) Mills, D. P.; Cooper, O. J.; Tuna, F.; McInnes, E. J. L.; Davies, E. S.; McMaster, J.; Moro, F.; Lewis, W.; Blake, A. J.; Liddle, S. T. *J. Am. Chem. Soc.* **2012**, *134*, 10047−10054.

(5) Fortier, S.; Wu, G.; Hayton, T. W. *J. Am. Chem. Soc.* **2010**, *132*, 6888−6889.

(6) Kosog, B.; La Pierre, H. S.; Heinemann, F. W.; Liddle, S. T.; Meyer, K. *J. Am. Chem. Soc.* **2012**, *134*, 5284−5289.

(7) Lam, O. P.; Franke, S. M.; Nakai, H.; Heinemann, F. W.; Hieringer, W.; Meyer, K. *Inorg. Chem.* **2012**, *51*, 6190−6199.

(8) La Pierre, H. S.; Meyer, K. *Inorg. Chem.* **2013**, *52*, 529−39.

(9) Brown, J. L.; Fortier, S.; Wu, G.; Kaltsoyannis, N.; Hayton, T. W. *J. Am. Chem. Soc.* **2013**, *135*, 5352−5355.

(10) Lewis, A. J.; Nakamaru-Ogiso, E.; Kikkawa, J. M.; Carroll, P. J.; Schelter, E. J. *Chem. Commun.* **2012**, *48*, 4977−4979.

(11) Lewis, A. J.; Carroll, P. J.; Schelter, E. J. *J. Am. Chem. Soc.* **2013**, *135*, 511−518.

(12) Lewis, A. J.; Carroll, P. J.; Schelter, E. J. *J. Am. Chem. Soc.* **2013**, *135*, 13185−13192.

(13) King, D. M.; Tuna, F.; McMaster, J.; Lewis, W.; Blake, A. J.; McInnes, E. J.; Liddle, S. T. *Angew. Chem., Int. Ed.* **2013**, *52*, 4921−4924.

(14) Edelstein, N.; Brown, D.; Whittaker, B. *Inorg. Chem.* **1974**, *13*, 563−567.

(15) Lukens, W. W.; Edelstein, N. M.; Magnani, N.; Hayton, T. W.; Fortier, S.; Seaman, L. A. *J. Am. Chem. Soc.* **2013**, *135*, 10742−10754.
(16) Hinatsu, Y.; Fujino, T.; Edelstein, N. *J. Solid State Chem.* **1992**, *99*, 182−188.
(17) Fortier, S.; Wu, G.; Hayton, T. W. *Inorg. Chem.* **2008**, *47*, 4752−4761.
(18) Seaman, L. A.; Fortier, S.; Wu, G.; Hayton, T. W. *Inorg. Chem.* **2011**, *50*, 636−646.
(19) Fortier, S.; Walensky, J. R.; Wu, G.; Hayton, T. W. *J. Am. Chem. Soc.* **2011**, *133*, 11732−11743.
(20) Seaman, L. A.; Wu, G.; Edelstein, N.; Lukens, W. W.; Magnani, N.; Hayton, T. W. *J. Am. Chem. Soc.* **2012**, *134*, 4931−4940.
(21) Graves, C. R.; Yang, P.; Kozimor, S. A.; Vaughn, A. E.; Clark, D. L.; Conradson, S. D.; Schelter, E. J.; Scott, B. L.; Thompson, J. D.; Hay, P. J.; Morris, D. E.; Kiplinger, J. L. *J. Am. Chem. Soc.* **2008**, *130*, 5272−5285.
(22) Graves, C. R.; Kiplinger, J. L. *Chem. Commun.* **2009**, 3831−3853.
(23) Mougel, V.; Biswas, B.; Pecaut, J.; Mazzanti, M. *Chem. Commun.* **2010**, *46*, 8648−8650.
(24) Mougel, V.; Pecaut, J.; Mazzanti, M. *Chem. Commun.* **2012**, *48*, 868−870.
(25) Fortier, S.; Wu, G.; Hayton, T. W. *Dalton Trans.* **2010**, *39*, 352−354.
(26) Bénaud, O.; Berthet, J.-C.; Thuéry, P.; Ephritikhine, M. *Inorg. Chem.* **2011**, *50*, 12204−12214.
(27) Thomson, R. K.; Graves, C. R.; Scott, B. L.; Kiplinger, J. L. *Dalton Trans.* **2010**, *39*, 6826−6831.
(28) Dormond, A.; El Bouadili, A.; Aaliti, A.; Moise, C. *J. Organomet. Chem.* **1985**, *288*, C1−C5.
(29) Bénaud, O.; Berthet, J.-C.; Thuéry, P.; Ephritikhine, M. *Inorg. Chem.* **2010**, *49*, 8117−8130.
(30) Fortier, S.; Brown, J. L.; Kaltsoyannis, N.; Wu, G.; Hayton, T. W. *Inorg. Chem.* **2012**, *51*, 1625−1633.
(31) Maynadié, J.; Berthet, J.-C.; Thuéry, P.; Ephritikhine, M. *Organometallics* **2007**, *26*, 4585−4591.
(32) Graves, C. R.; Vaughn, A. E.; Schelter, E. J.; Scott, B. L.; Thompson, J. D.; Morris, D. E.; Kiplinger, J. L. *Inorg. Chem.* **2008**, *47*, 11879−11891.
(33) Ryan, J. L. *J. Inorg. Nucl. Chem.* **1971**, *33*, 153−177.
(34) Bart, S. C.; Anthon, C.; Heinemann, F. W.; Bill, E.; Edelstein, N. M.; Meyer, K. *J. Am. Chem. Soc.* **2008**, *130*, 12536−12546.
(35) Fortier, S.; Kaltsoyannis, N.; Wu, G.; Hayton, T. W. *J. Am. Chem. Soc.* **2011**, *133*, 14224−14227.
(36) Rao, K. R.; Trevino, S. F.; Prask, H.; Mical, R. D. *Phys. Rev. B* **1971**, *4*, 4551−4555.
(37) Straka, M.; Patzschke, M.; Pyykkö, P. *Theor. Chem. Acc.* **2003**, *109*, 332−340.
(38) Denning, R. Electronic Structure and Bonding in Actinyl Ions. In *Complexes, Clusters and Crystal Chemistry;* Springer: Berlin/Heidelberg, 1992; Vol. *79*, pp 215−276.
(39) Brennan, J. G.; Andersen, R. A. *J. Am. Chem. Soc.* **1985**, *107*, 514−516.
(40) Rosen, R. K.; Andersen, R. A.; Edelstein, N. M. *J. Am. Chem. Soc.* **1990**, *112*, 4588−4590.
(41) Cooper, O. J.; Mills, D. P.; McMaster, J.; Tuna, F.; McInnes, E. J.; Lewis, W.; Blake, A. J.; Liddle, S. T. *Chem.—Eur. J.* **2013**, *19*, 7071−7083.
(42) Gourier, D.; Caurant, D.; Arliguie, T.; Ephritikhine, M. *J. Am. Chem. Soc.* **1998**, *120*, 6084−6092.
(43) Gourier, D.; Caurant, D.; Berthet, J. C.; Boisson, C.; Ephritikhine, M. *Inorg. Chem.* **1997**, *36*, 5931−5936.
(44) Meyer, K.; Mindiola, D. J.; Baker, T. A.; Davis, W. M.; Cummins, C. C. *Angew. Chem., Int. Ed.* **2000**, *39*, 3063−3066.
(45) Nocton, G.; Horeglad, P.; Vetere, V.; Pécaut, J.; Dubois, L.; Maldivi, P.; Edelstein, N. M.; Mazzanti, M. *J. Am. Chem. Soc.* **2009**, *132*, 495−508.
(46) Castro-Rodríguez, I.; Meyer, K. *Chem. Commun.* **2006**, 1353−1368.
(47) Baker, J.; Scheiner, A.; Andzelm, J. *Chem. Phys. Lett.* **1993**, *216*, 380−388.
(48) Kaupp, M.; Bühl, M.; Malkin, V. G. *Calculation of NMR and EPR Parameters: Theory and Applications;* John Wiley & Sons: Hoboken, NJ, 2006.
(49) Avens, L. R.; Bott, S. G.; Clark, D. L.; Sattelberger, A. P.; Watkin, J. G.; Zwick, B. D. *Inorg. Chem.* **1994**, *33*, 2248−2256.
(50) Turner, H. W.; Andersen, R. A.; Zalkin, A.; Templeton, D. H. *Inorg. Chem.* **1979**, *18*, 1221−1224.
(51) Bruker. *SAINT;* Bruker AXS, Inc.: Madison, Wisconsin, USA, 2009.
(52) Bruker. *SHELXTL;* Bruker AXS, Inc.: Madison, Wisconsin, USA, 2009.
(53) Sheldrick, G. M. *TWINABS;* University of Gottingen: Gottingen, Germany, 2008.
(54) Sheldrick, G. M. *SADABS;* University of Gottingen: Gottingen, Germany, 2007.
(55) Sheldrick, G. M. *Acta Crystallogr.* **2008**, *A64*, 112−122.
(56) Gaussian 09, Revision C.01. Full reference given in Supporting Information.
(57) Küchle, W.; Dolg, M.; Stoll, H.; Preuss, H. *J. Chem. Phys.* **1994**, *100*, 7535−7542.
(58) Cao, X. Y.; Dolg, M. *J. Mol. Struct. (THEOCHEM)* **2004**, *673*, 203−209.
(59) Gorelsky, S. I.; Lever, A. B. P. *J. Organomet. Chem.* **2001**, *635*, 187−196.
(60) Gorelsky, S. I. *AOMix: Program for Molecular Orbital Analysis,* http://www.sg-chem.net/, Version 6.54, 2011.